

Revealing the secrets of high performance lead-free CsSnCl_3 based perovskite solar cell: A dive into DFT and SCAPS-1D numerical insights



Okba Saidani^{a, **}, Abderrahim Yousfi^a, D.P. Samajdar^b, Xueqing Xu^c, Taye Biniyam Zemene^c, Sagar Bhattacharai^d, M Khalid Hossain^e, Girija Shankar Sahoo^{f,*}

^a ETA Laboratory, Department of Electronics, Faculty of Sciences and Technology, University of Mohamed El Bachir El Ibrahimi, Bordj Bou Arréridj, 34030, Algeria

^b Dept. of ECE, Indian Institute of Information Technology, Design & Manufacturing, Madhya Pradesh, 482005, India

^c Key Laboratory of Renewable Energy, Guangdong Provincial Key Laboratory of New and Renewable Energy Research and Development, Guangzhou Institute of Energy Conversion, Chinese Academy of Sciences, Guangzhou, 510640, PR China

^d Technology Innovation & Development Foundation, Indian Institute of Technology Guwahati, Guwahati, Assam, 781039, India

^e Institute of Electronics, Atomic Energy Research Establishment, Bangladesh Atomic Energy Commission, Dhaka, 1349, Bangladesh

^f School of Electronics Engineering (SENSE), Vellore Institute of Technology, Vandalur-Kellambakkam Road, Chennai, Tamil Nadu, 600127, India

ARTICLE INFO

Keywords:

CsSnCl_3
DFT
PCE
Defect density
Lead free solar cell
WIEN2k
SCAPS-1D

ABSTRACT

In this study, a CsSnCl_3 /CBTS based hetero structure solar cell is proposed by incorporating effective ETLs like CBTS and HTLs built on C_{60} . At first, electrical and optical properties of CsSnCl_3 is determined with the help of DFT study. Those parameters are incorporated in SCAPS-1D to design the proposed solar cell. Numerical analysis demonstrates that heterostructures consisting of ITO/ C_{60} / CsSnCl_3 /CBTS/Au display remarkable photoconversion efficacy. In addition, the impact of CsSnCl_3 thickness, series resistance, light conversion efficiency, also working temperature is investigated additionally to optimize the cell performance. Furthermore, the composed impacts of thickness of absorber and ETL, defect density, electron affinity (eV), absorption thickness, and doping are also explored. The SCAPS-1D simulation results, which show an ideal open-circuit voltage of 1.18 V, a short-circuit current density of 22.22 mA/cm^2 , a fill factor of 87 %, and an overall efficiency of 20.5 %, are in good agreement with both simulated and experimental data published in the literature. This thorough simulation analysis provides insightful information and identifies a viable path for future CsSnCl_3 -based solar cell development.

1. Introduction

Metal halide perovskites (MHPs) have revolutionized the landscape of photoelectric materials science, especially in the realm of solar cell applications, boasting a general formula of ABX_3 [1]. Here, A commonly represents a monovalent cation (e.g., MA^+ , FA^+ , Cs^+), B stands as a divalent cation (e.g., Pb^{2+} or Sn^{2+}), and X functions as a halide anion (e.g., Cl^- , Br^- , I^-). The fundamental structure of MHPs involves the coordination of the B-site cation with six halide anions X, forming $[\text{BX}_6]^{4-}$ octahedra [2]. In recent years, MHPs have garnered significant attention in the optoelectronic field, thanks to their noteworthy characteristics, including cost-effectiveness, prolonged charge diffusion, and high carrier mobility. Notably, the power conversion efficiency (PCE) of MHPs has experienced a remarkable surge from 3.8 % to 25.2 % within a

decade [3], positioning them as highly promising candidates for various applications, such as photovoltaic devices, photodetectors, light-emitting diodes, and lasers [4,5]. Despite their remarkable characteristics, the application of most metal halide perovskites (MHPs) has been hindered by the toxicity of lead [6,7]. This has prompted an ongoing quest in the solar cell field for photo absorbers that are both non-toxic and highly efficient. Tin halide perovskites have emerged as a promising alternative with lower toxicity compared to lead halide perovskites, capitalizing on the similar electronic structure of Sn to Pb [8]. Additionally, Sn-based perovskites offer advantages such as a tunable direct bandgap and high absorption capabilities for solar energy conversion [9,10]. Among these alternatives, CsSnCl_3 perovskites, known for their impressive dielectric properties and ductility, have received limited attention in relevant studies. A comprehensive understanding of

* Corresponding author.

** Corresponding author.

E-mail addresses: okbasaidani3@gmail.com, okba.saidani@univ-bba.dz (O. Saidani), sahoo.girija26@gmail.com, girija.shankarsahoo@vit.ac.in (G.S. Sahoo).

their electronic structure and dielectric properties is pivotal for assessing and optimizing their performance [11]. Numerous research initiatives have explored the synthesis of more stable CsSnCl_3 perovskites, and various groups have investigated metal doping to narrow the bandgap and enhance absorptivity. Essentially, these endeavors aim to unlock the full potential of CsSnCl_3 perovskites as a viable and environmentally friendly option for advanced solar cell technologies [12,13]. The development of CsSnCl_3 perovskite solar cells represents a crucial milestone in the pursuit of sustainable and efficient photovoltaic technologies. Serving as a lead-free substitute for conventional perovskite materials, CsSnCl_3 perovskite has garnered substantial attention for its capacity to revolutionize solar energy harvesting. With an inherent abundance of cesium and tin, this innovative perovskite not only addresses environmental concerns associated with lead-based counterparts but also offers prospects for increased stability and tunable optoelectronic properties [14]. The confluence of these attributes positions CsSnCl_3 perovskite solar cells as promising contenders in the ongoing quest for clean and renewable energy sources [15,16]. This study's primary aim is to identify a dependable and efficient CsSnCl_3 -based solar cell (SC) through numerical simulations, serving as an initial assessment before engaging in resource-intensive experimental characterization processes. The investigation systematically explores the impact of CsSnCl_3 absorber layer thickness, carrier (donor/acceptor) density, and defect density, as well as the influence of ETLs and HTL thickness on the overall design. Global design optimization is performed to discern optimal configurations. Additionally, the study extends to the effects of operating temperature, series resistance, and shunt resistance on the electrical parameters of the optimized cells, along with the corresponding quantum efficiency. This comprehensive exploration aims to identify parameters contributing to potential shortcomings in Sn-based solar cells and propose viable solutions. The proposed architecture is illustrated in Fig. 1. The simulations, conducted using SCAPS-1D, are validated by comparing results with recent studies. These validated simulation outcomes provide valuable insights into the potential of CsSnCl_3 -based perovskites in contemporary photovoltaic and optoelectronic devices, highlighting their environmentally friendly characteristics.

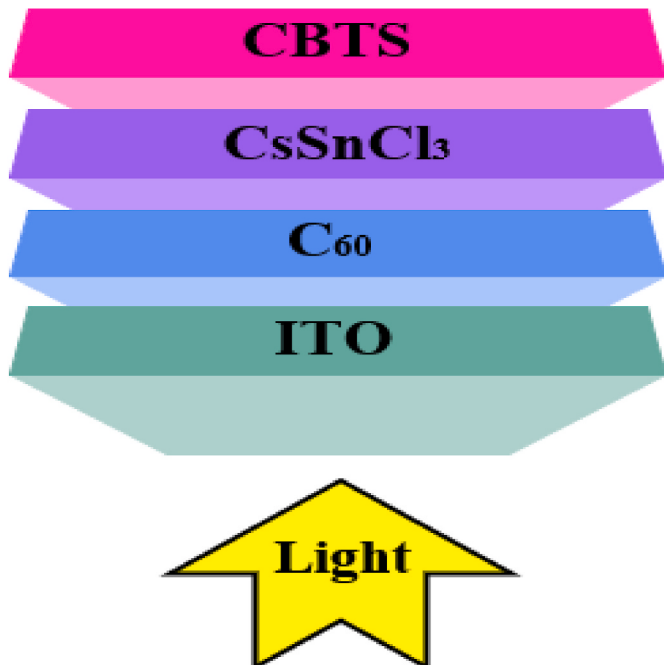


Fig. 1. Design configuration of the CsSnCl_3 -based PSC.

2. Device settings and simulation process

The suggested design adopts three-part structure consisting of the electron transport layer (ETL), the doped p-type perovskite layer, and the hole transport layer (HTL) [17,18]. When exposed to light, this setup generates excitons, Particle pairs in a confined energy state, primarily within the perovskite layer [19,20]. Due to their comparatively long diffusion lengths, these excitons, which are made up of holes and electrons, can migrate into the n-region for holes and the p-region for electrons [21,22]. These excitons are separated at the interface of the perovskite layer and the ETL [23,24]. Next, the electrons are moved to the appropriate electrode via the ETL, and the holes are effectively moved through the HTL [25,26]. Excitons are dissociated and transported more easily thanks to the intrinsic electric field that exists between the perovskite layer and the ETL (or HTL). The functioning of the solar cell as a whole is influenced by this electric field, which speeds up the passage of electrons and holes towards their corresponding contacts [27]. We included advanced materials in our calculations for both the ETL and HTL layers, namely copper barium thiostannate (CBTS) for the HTL and (C_{60}) for the ETL [28,29]. The simulation results demonstrated that solar cell structures composed of indium tin oxide (ITO)/ C_{60} / CsSnCl_3 /CBTS/Au shows remarkably Excellent effectiveness of photoconversion, as illustrated in Fig. 1.

The widely utilized SCAPS-1D simulator, developed at the University of Gent, enables the numerical solution of fundamental 1-Dimensional semiconductor equations under steady-state conditions by considering all of the above-mentioned parameters [30,31]. SCAPS-1D customization allows users to explore and calculate results, shedding light on carrier density, carrier transit mechanisms, electric field distribution, and recombination profiles. The simulation incorporates the Poisson formula to describe the relationship between the electric field (E) and space charge density (ρ) in a p-n junction. An essential aspect of achieving optimal efficiency involves investigating the impact of defect concentrations on solar cell performance. High defect density (N_t) resulting from inferior film quality tends to induce charge recombination in the light absorber layer [32,33]. The analysis of defect density on cell performance involves the application of the Shockley-Read-Hall recombination model (SRH), which represents the recombination of holes from the valence band (V_B) and electrons from the conduction band (C_B) via trap states [34,35]. This comprehensive exploration provides valuable insights into the intricate interplay between defect concentrations and the performance of perovskite-based solar cells. Photocarrier generation and immediate recombination in the absorber layer, influenced by defect concentrations, are critical considerations. The efficiency (η) of solar cells is intricately linked to the morphology and quality of perovskite films. These simulations were run at typical circumstances, which include 300 K ambient temperature and AM1.5G illumination. In addition, as shown in Table 1, we carefully established the simulation settings for the CsSnCl_3 , HTL, and ETL layers [36,37]. In the simulation groundwork, these characteristics are essential for precisely predicting the behavior and performance of the solar cell.

3. Results and discussion

3.1. Structure properties of the cubic CsSnCl_3

The cubic phase of CsSnCl_3 a halide perovskite with space group $Pm\bar{3}m$ (221) is shown in Fig. 2(a). The unit cell of the CsSnCl_3 contains five atoms in one formula unit. An atom in the unit cell, the Cs atom is placed in the corner, the Sn atom is arranged at the center, and halide atom Cl is located at face centered with the Wyckoff position of 1a (0,0,0), 1b (0.5, 0.5, 0.5) and 3c (0.5, 0.5, 0) respectively [38]. The relaxed crystal structure was obtained with the Birch-Muranghan equation. The calculated energy versus volume curve of CsSnCl_3 perovskite is illustrated in Fig. 2(b). The optimized ground state energy (E_0) is -30708.369 Ryd and Volume (V_0) is 1208.98 (a.u) 3 of the relaxed

Table 1
Input values of CsSnCl_3 , ETL and HTL.

Parameters	Terms	ITO	ETL (C_{60})	PVK (CsSnCl_3)	HTL (CBTS)
$d(\mu\text{m})$	Thickness	0.5	0.6	0.5	0.8
$\chi(\text{eV})$	Electron Affinity (eV)	4.1	3.9	3.95	3.6
$E_g(\text{eV})$	Band gap	3.5	1.7	1.52	1.9
ϵ_r	Relative	9	4.2	29.4	5.4
	Permittivity				
$N_c(1/\text{m}^3)$	Effective Density Of States (C_B)	2.2×10^{18}	1×10^{19}	1.8×10^{18}	2.2×10^{18}
$N_v(1/\text{m}^3)$	Effective Density of States (V_B)	3.8×10^{18}	5×10^{20}	2.2×10^{18}	1.8×10^{19}
$\mu_n(\text{cm}^2/\text{Vs})$	Electron Mobility	20	100	2	30
$\mu_p(\text{cm}^2/\text{Vs})$	Hole Mobility	10	25	2	10
$N_A(1/\text{cm}^3)$	Acceptor Density N_A	5	5	5×10^{15}	1×10^{18}
$N_D(1/\text{cm}^3)$	Donor Density N_D	10^{17}	1×10^{20}	5	5
N_t	Defect Density	10^{14}	1×10^{15}	1×10^{14}	1×10^{14}

structure of CsSnCl_3 .

of the CsSnCl_3 crystal structure.

Additionally, the stability of the crystal structure ABX_3 is also determined by Goldschmidt's tolerance factor (t) and octahedral factor (μ) and expressed by the equation given below [39]:

$$t = \frac{r_A + r_X}{\sqrt{2}(r_B + r_X)} \quad (1)$$

$$\mu = \frac{r_A}{r_B} \quad (2)$$

where, r_A , r_B , and r_X are the radii of the Cs, Sn, and Cl respectively. For the stable cubic perovskite, the t value must be in the range of 0.8–1.0 and the μ value should be 0.4 to 0.7. The calculated values of t and μ of are xx and yy respectively. This value indicates that Cubic CsSnCl_3 is the stable perovskite for use as an absorber in the PSC.

3.2. Study of the electronic properties of the CsSnCl_3

The electronic band structure is fundamental to semiconductor physics and materials properties. It shows electron energy levels for electrons in semiconductor materials. In this, we analyzed the electronic band structure, density of states (DOS), and electron density of CsSnCl_3 , which are plotted in Fig. 3(a) and (b), respectively. All the electronic properties of CsSnCl_3 are calculated and analyzed through the TB-mBJ approximation in WIEN2k. The minimum and maximum points in the conduction band (CBM) and valence band (VBM) were found at the R point in the band structure, where zero energy is indicated at the Fermi level. The TB-mBJ calculated bandgap (E_g) of CsSnCl_3 is 1.57 eV, which is direct bandgap in nature and is suitable for absorber in the solar cell application. The value of the band gap is considered to be one of the most important characteristics for determining the light-absorbing properties of materials used in solar cells [39]. The contributions of the electronic states to the conduction band (C_B) and valence band (V_B) are represented by the total density of State (T-DOS) as shown in Fig. 3(b) a vertical dotted line with that designates the Fermi level at zero energy level. The DOS graph shows that Cs contribute less to T-DOS. Which contributed to the Cl atom is minimal to the valence band. The minimum part of the conduction band is influenced by the Sn and Cl

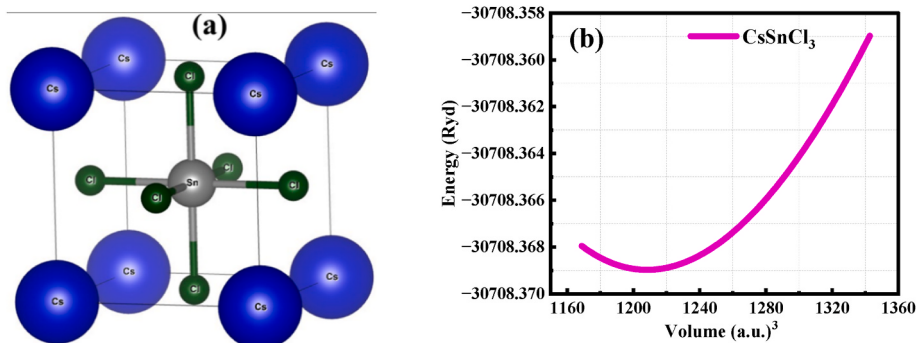


Fig. 2. (a) Generated Crystal unit cell and (b) energy volume optimization.

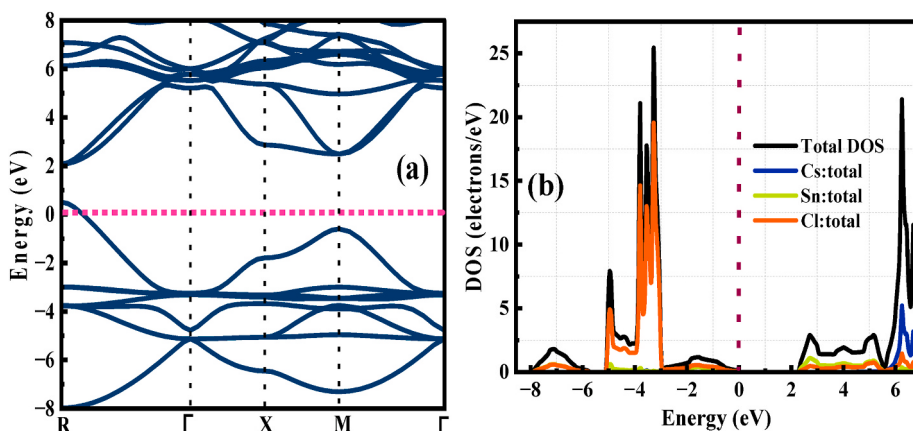


Fig. 3. (a) The electronic band structure and (b) T-DOS of the cubic crystal structure CsSnCl_3 .

atoms. As a result, the bandgap of CsSnI_3 is mostly contributed by the interaction of Sn and I atoms, emphasizing their important roles in regulating the material's electrical characteristics.

3.3. Study of the optical properties of the CsSnCl_3

Investigating the optical properties of perovskite CsSnCl_3 is important because it reveals how the material reacts to electromagnetic radiation within the context of DFT. Fig. 4(a) shows the calculated dielectric function. The dielectric function is a crucial term in the investigation of a material's reaction to an incident electromagnetic disturbance, giving important information about how the material interacts with external electromagnetic radiation. It is a complex function typically denoted as (ω) , where ω represents the angular frequency of the incident electromagnetic field and is expressed by the equation given below [40]:

$$\varepsilon(\omega) = \varepsilon_1(\omega) + i\varepsilon_2(\omega) \quad (3)$$

where $\varepsilon_1(\omega)$ and $\varepsilon_2(\omega)$ represent the real part and imaginary of the dielectric function. The actual portion, $\varepsilon_1(\omega)$, defines the material's electrical energy storage and polarization response to an external electric field. It indicates light propagation by being related to the material's refractive index. When the incident light's energy increases, $\varepsilon_1(\omega)$ of perovskite grows and reaches a maximum at 2.4 eV and then starts to decline. The static value of $\varepsilon_1(0)$ at zero energy is given as 3.6 eV that is, the polarization peaks in the frequency range and then falls to its lowest point. While $\varepsilon_2(\omega)$ dielectric function, which indicates the absorbed radiation by the compound, has noticeable peaks in the energy range of 3.4–5 eV. It is worth noting that $\varepsilon_2(\omega)$ remains zero until absorption begins as a result of the photon energy exceeding the band gap energy.

In Fig. 4 (b), the absorption coefficient $\alpha(\omega)$ of the order 10^{-4} cm^{-1} is shown against photon energy from 0 to 12 eV. There is no absorption at the static value. However, as photon energy increases, absorption occurs

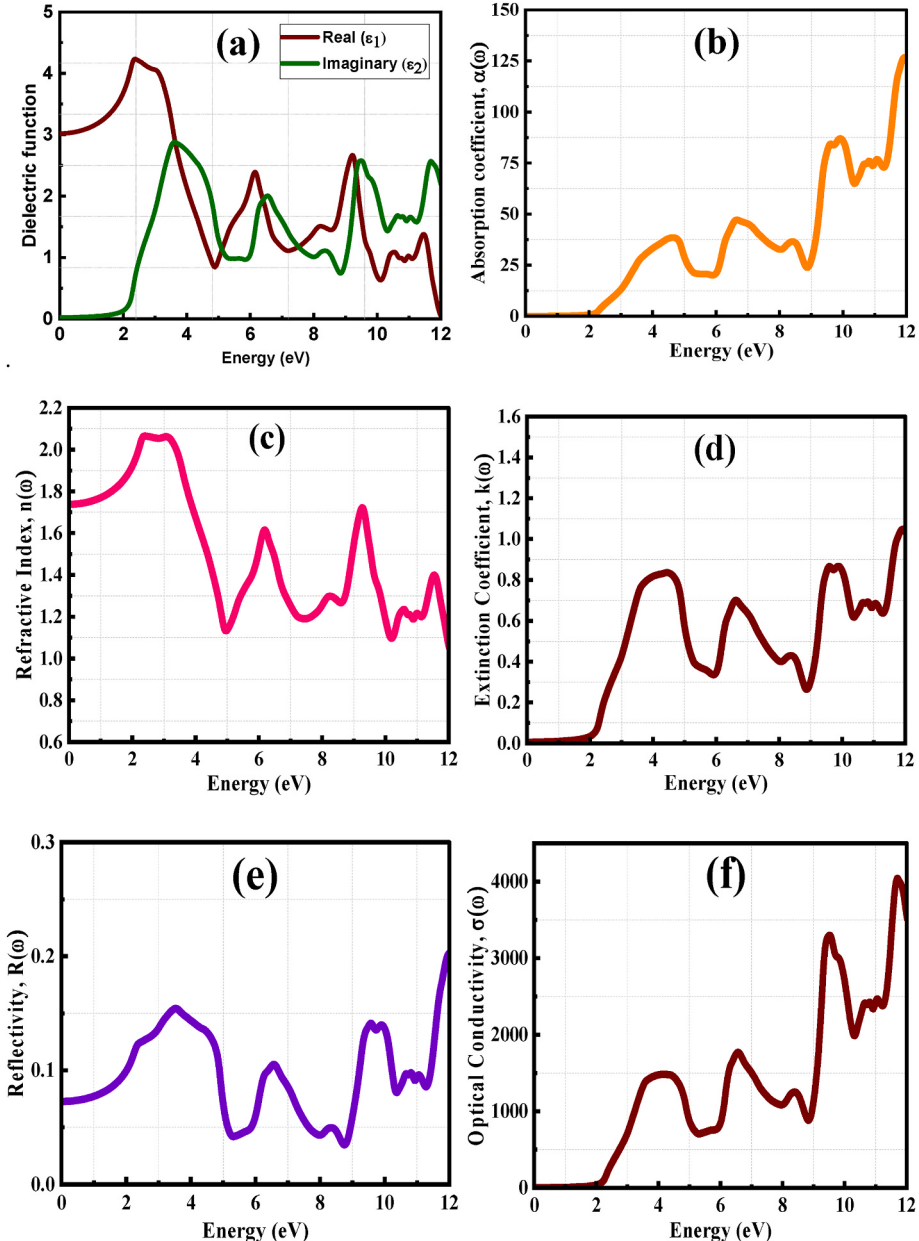


Fig. 4. The optical properties of CsSnCl_3 are presented as (a) The imaginary and real components of the dielectric function, (b) absorption coefficient, (c) refractive index, (d) extinction coefficient, (e) reflectivity (f) optical conductivity.

at 1.6 eV and the furthermore, as the energy level increased, the absorption values increased. The higher pick in the visible range is observed at photon energy 4.6 eV. The explicit demonstration of light photon absorption is achieved by employing the extinction coefficient $k(\omega)$ depending on the imaginary dielectric function $\epsilon_2(\omega)$, which is computed using the equation [41]:

$$\alpha = \frac{4\pi k}{\lambda} \quad (4)$$

The complex refractive index is an optical property that defines how light interacts with a substance. The frequency of the incident light beam determines it. The complex refractive index consists of the real and composed portions as expressed below [42]:

$$\eta(\omega) = n(\omega) + k(\omega) \quad (5)$$

where $n(\omega)$ represents the real component of the complex refractive index is referred to as the reflective index, while $k(\omega)$ signifies the

imaginary part of the complex refractive index and is referred to as the extinction coefficient. Which is shown in Fig. 4(c) and (d). The static function value of the static reflective index $n(0)$ at zero energy is 1.73. Beginning at the static frequency limit, we observed an increase in the $n(\omega)$ values of all substances, with several peaks appearing across different energy ranges. CsSnCl_3 showed the largest peak, at 2.38551 eV. The extinction coefficient, $k(\omega)$, provides insight into how optical energy is absorbed within an optical material during light transmission. Studies have demonstrated comparable patterns between the dielectric function and the real part of the refractive index. Similarly, the $n(\omega)$ and the $k(\omega)$ of the dielectric function have comparable properties. Additionally, the $k(\omega)$ values increased as the energy level increased as well, as illustrated in Fig. 4(d). The light reflection from a compound's surface is very significant for the application of materials. The optical reflectivity of different materials can be calculated by using the complex refractive index, as shown in Fig. 4(e). Upon analyzing the chemicals in question, it was discovered that the range of low to high energy corresponds to the maximum reflectivity. Notably, CsSnCl_3 has the maximum

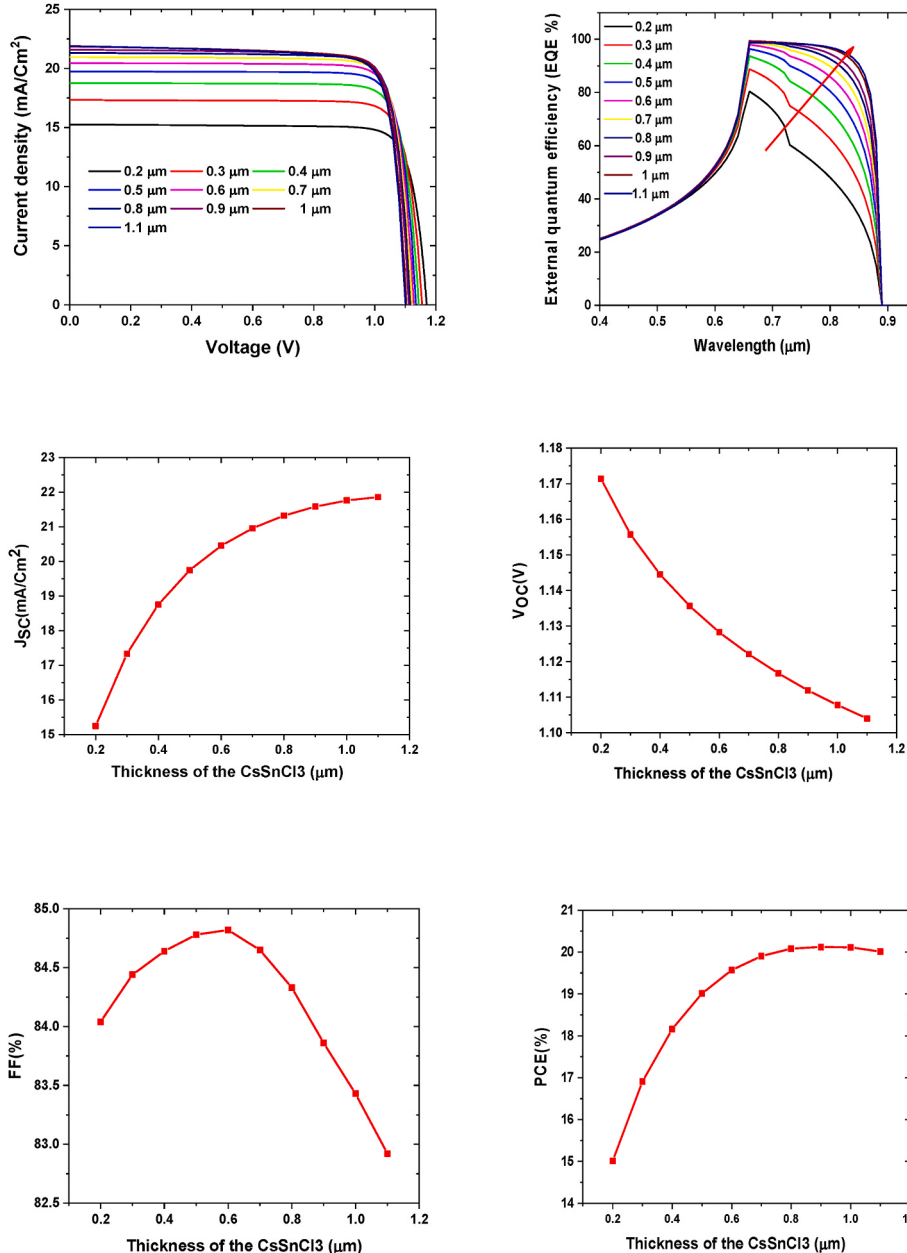


Fig. 5. Effect of perovskite layer (CsSnCl_3) thickness on J-V; EQE; V_{OC} ; J_{SC} ; FF; PCE.

reflectance precisely at 3.5 eV in the visible range. Investigating the optical conductivity, $\sigma(\omega)$ for predicted stable halide perovskite compounds CsSnCl_3 is crucial, as shown in Fig. 4(f). The highest peaks of $\sigma(\omega)$ rises in the visible range at 4.28 eV. The maximum peak is observed at higher photon energies.

3.4. Effect of the CsSnCl_3 thickness

Variations in the PVK thickness directly impact the IV characteristics, including J_{SC} , V_{OC} , and FF. Examination of EQE spectra offers insights into the solar cell's wavelength-dependent response, with changes in PVK thickness influencing the EQE profile. Essentially, one of the most important aspects of device design is optimizing the thickness of the PVK layer, necessitating a delicate balance to maximize light absorption and carrier generation while minimizing losses from recombination, resistive losses, and other factors. Simulations have an important place in determining the optimal PVK layer thickness to produce high-performance solar cells. A thicker PVK layer has the potential to enhance light absorption, leading to increased photon harvesting within the material and, consequently, higher J_{SC} and overall improved device performance (refer to Fig. 5) [43,44]. An important factor affecting the rates of charge carrier production and recombination is the thickness of the PVK layer. Striking a balance is essential to prevent excessive carrier recombination, which could result in a reduction in V_{OC} and FF [45,46]. The increased value of perovskite layer thickness gives birth to recombination, charge transport issue, increased defect density, electric field distribution issues, optical absorption saturation and series resistance in the solar cell. These are the prime cause of the decreasing V_{OC} with increasing perovskite thickness. As the high value of $V_{OC} = 1.175$ V is obtained at perovskite layer thickness of 0.2 μm ; while a low value of $V_{OC} = 1.11$ V is obtained at perovskite layer thickness of 1.1 μm . An increase in the PVK layer thickness extends the optical path length for photons within the absorber material. This extended optical path length,

coupled with enhanced light absorption, contributes to a higher EQE across a broader spectral range (refer to Fig. 5) [47,48].

3.5. Effect of series resistance

In Fig. 6, we examine the influence of series resistance (R_s) on photovoltaic (PV) outputs across the 0–6 $\Omega\text{-cm}^2$ range, while maintaining a constant shunt resistance (R_{SH}) of $10^5 \Omega\text{-cm}^2$. The V_{OC} and J_{SC} show minimal changes as R_s increases, but the FF experiences a notable decrease from approximately 85 %–75 %. Consequently, the PCE also declines from around 19 %–17 % as R_s goes from 0 to 6 $\Omega\text{-cm}^2$. It's worth noting that a highly conductive indium tin oxide (ITO) layer tends to mitigate the introduction of series resistance for non-ohmic contacts. The series resistance (R_s) in a solar cell encompasses resistances from various active materials, including those at the interface between metal contacts and semiconductors [49,50]. While there is no overall current flow through R_s , it can potentially impact V_{OC} . Increased R_s causes FF to drop significantly, resulting in reduced PCE due to increased power loss. Consequently, identifying optimal R_s values is crucial for achieving high performance, such as a PCE of 19 %, in specific architectures like ITO (0.5 μm)- C_60 (0.5 μm)- CsSnCl_3 (0.5 μm)-CBTS (0.5 μm). This emphasizes the importance of carefully managing series resistance to optimize the overall performance of solar cell structures [51].

3.6. Impact of shunt resistance

The impact of shunt resistance (R_{SH}) on several photovoltaic (PV) output parameters is examined in Fig. 7, containing V_{OC} , J_{SC} , FF, and PCE, inside of 10^1 to $10^7 \Omega\text{-cm}^2$, while maintaining a fixed series resistance at $1 \Omega\text{-cm}^2$. Notably, for the ITO ETL configuration, V_{OC} , J_{SC} , and FF exhibit substantial increases from approximately 1.1 to 1.136 V, 19.6–19.8 mA/cm^2 , and 55 %–85 %, respectively, as R_{SH} rises from 10^1 to $10^7 \Omega\text{-cm}^2$. It is observed that beyond $10^3 \Omega\text{-cm}^2$, increments in R_{SH}

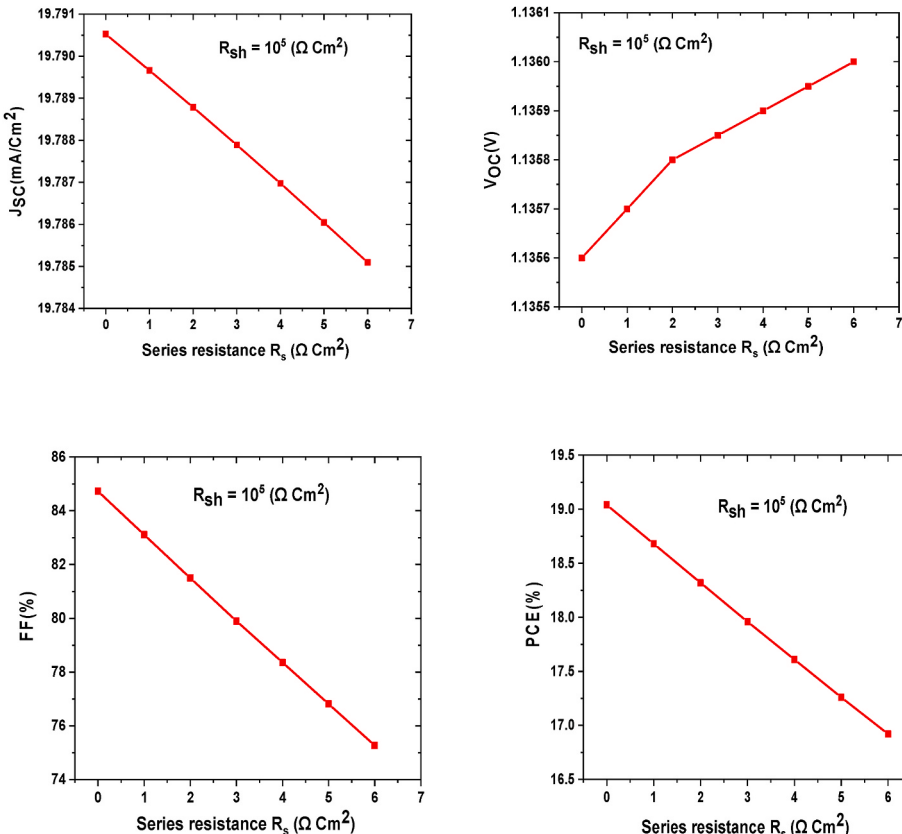


Fig. 6. Result of R_s on V_{OC} ; J_{SC} ; FF; PCE at an $R_{SH} = 10^5 \Omega\text{-cm}^2$.

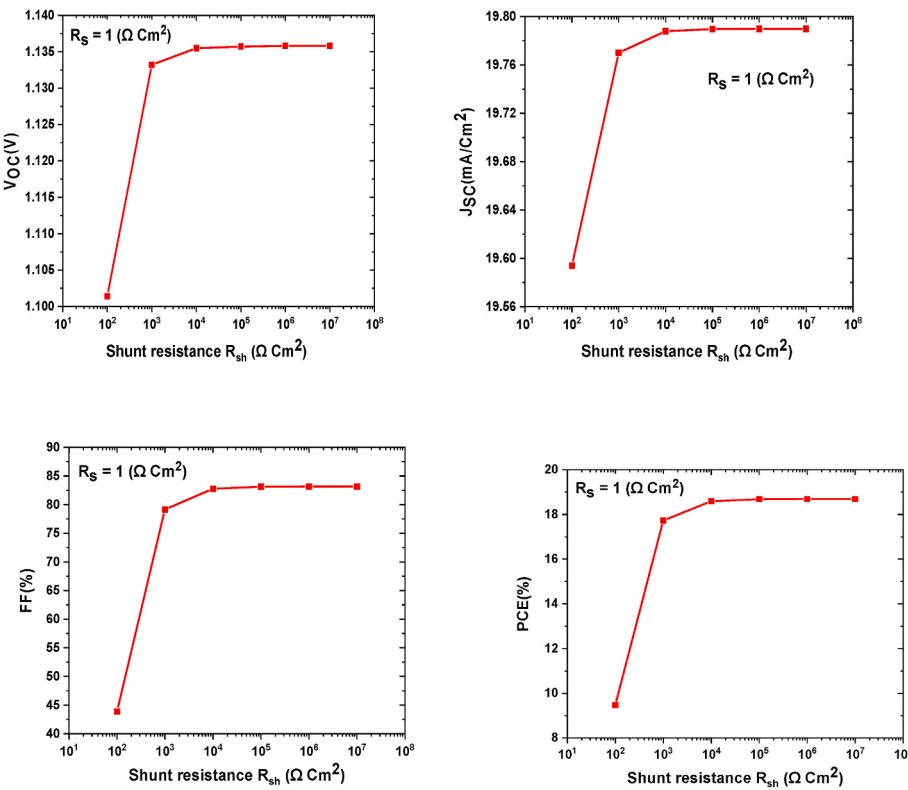


Fig. 7. Consequence of R_{SH} on V_{OC} ; J_{sc} ; FF; PCE.

lead to saturation in V_{OC} , J_{sc} , FF, and PCE. Shunt resistance (R_{SH}) is associated with manufacturing defects and material impurities, serving as a lower-resistance path across the p-n junction, facilitating the flow of photocurrent with reduced hindrance [52]. Simulation results highlight a noticeable impact of R_{SH} on both FF and PCE. Notably, the CsSnCl₃-based solar cell demonstrates its maximum PCE, reaching approximately 19 %, at an R_{SH} of $10^3 \Omega\text{-cm}^2$, in line with previous research findings [53].

3.7. Effect of temperature

In Fig. 8, we examine the impact of working temperature (T) ranging from 260 to 440 K on the photovoltaic performance. Notably, V_{OC} and FF undergo significant decreases, shifting from approximately 1.18 to 0.95 V and 87 %-78 %, respectively. Consequently, the power conversion efficiency (PCE) experiences a sublinear reduction from 20.5 % to 16.5 %, while a substantial increment is observed in J_{sc} as T increases from 260 to 440 K. This pattern is also visible in the external curve of quantum efficiency. An increase in J_{sc} results from the cell producing more excitons when the temperature rises. The reduced PCE at higher temperatures is attributed to the thermal excitation of carriers, which results in a shorter diffusion length and potential deformation stress. Simulation results underscore that the ITO (0.5 μm)-C₆₀ (0.5 μm)-CsSnCl₃ (0.5 μm)-CBTS (0.5 μm) heterojunction solar cell demonstrates the uppermost performance, achieving a PCE of approximately 19.5 % at atmospheric temperature. This aligns with findings from previous reports [54].

3.8. Effect of ETL' N_D

In Fig. 9, we analyze the impact of doping concentration (N_D) ranging from 10^{14} to 10^{19} cm^{-3} on photovoltaic performance. Initially, as N_D increases, J_{sc} experiences a rise. However, with further increases in N_D , J_{sc} undergoes a drastic decrease. This phenomenon is attributed to the reduction in electron mobility with increasing concentration,

consequently impacting J_{sc} negatively. Simultaneously, other parameters such as V_{OC} , FF, and PCE exhibit an increment, shifting from 1.1725 to 1.1805 V, 78 %-85.5 %, and 18.2 %-19.9 %, respectively. Despite the decline in J_{sc} , the increase in V_{OC} and FF contributes to a higher overall power conversion efficiency (PCE).

3.9. Affinity effect of ETL film

The difference in the affinity of the ETL has a major impact on a perovskite solar cell's performance. The energy level alignment between the perovskite absorber layer and the ETL is referred to in this context as affinity. Boosting charge extraction, lowering recombination, and improving PSC performance all depend on optimizing the affinity of the ETL layer. This optimization aims to maximize key parameters such as V_{OC} , J_{sc} , FF, and PCE, ultimately contributing to the efficiency and reliability of the solar cell technology. Affinity affects the mobility and transport of charge carriers (electrons) through the ETL. A well-matched affinity facilitates smooth transport, reducing resistive losses. Improved charge carrier transport contributes to a higher J_{sc} and FF, both crucial for enhancing the PCE. Affinity effects the V_{OC} of the solar cell. Optimal energy level alignment allows for an upper V_{oc} by minimizing energy losses during charge extraction. In cases of appropriate affinity, the V_{oc} tends to increase, contributing to enhanced overall performance. From Fig. 10 it is concluded that with an affinity value of 4.05 eV, the proposed structure shows a highest efficiency of 20.5 %.

3.10. Impact t of absorber acceptor doping

One important factor that affects a solar cell's electrical and optical characteristics is the concentration of acceptor in the absorber material. A precise adjustment of this concentration is required to maximize the performance of the solar cell, efficiency, and stability. Higher acceptor concentrations can increase the hole concentration, enhancing electrical conductivity. Acceptor dopants can influence the bandgap of the CsSnCl₃ material. This is important for tailoring the absorption spectrum

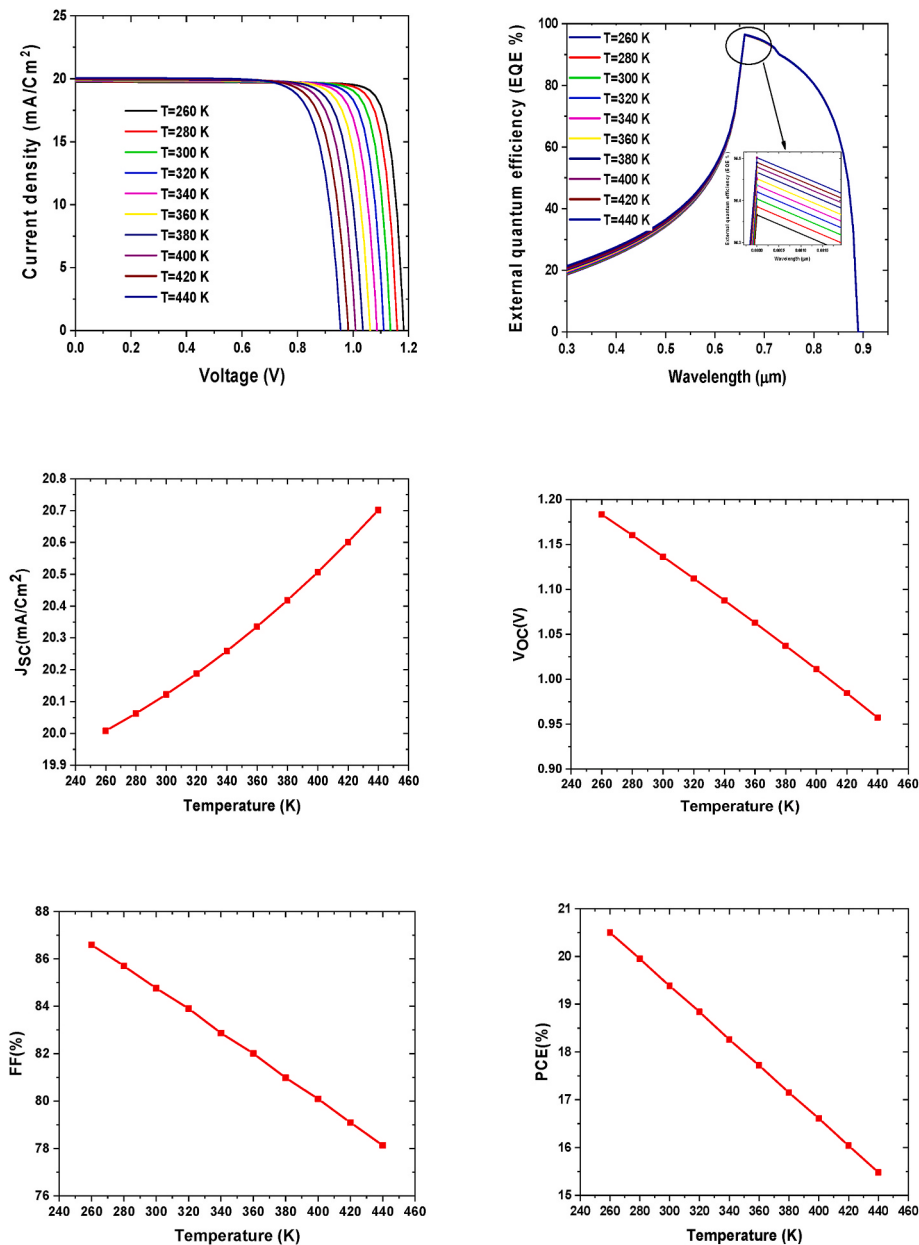


Fig. 8. Temperature influence from 260 to 440 K on J-V; EQE; V_{OC}; J_{sc}; FF; PCE.

to match the solar spectrum, maximizing the solar energy's conversion to power. The concentration of the acceptor influences the solar cell's V_{OC}. Higher acceptor concentrations can impact the material's energy levels, affecting the voltage output. Optimizing acceptor concentration is crucial for achieving the desired V_{OC} and maximizing the solar cell's effectiveness. Acceptors can reduce the likelihood of electron-hole recombination by capturing excess electrons and creating localized potential energy wells. Proper control of acceptor concentration helps minimize recombination losses, increasing the solar cell's total efficiency. But with increasing doping concentration the mobility decreases so the J_{sc}. All of this can be seen from Fig. 11. With an optimized doping concentration a highest concentration of 20.8 % can be achieved.

3.11. Effect of Affinity x of absorber

We've previously emphasized the significance of affinity, and now we delve into its pivotal role in optimizing perovskite solar cells. Achieving an optimal affinity for the PVK film is essential for enhancing

charge extraction, diminishing recombination, and improving the solar cell's overall performance. This strategic optimization targets key parameters, including V_{OC}, J_{sc}, FF, and PCE, with the ultimate goal of boost up the PCE and reliability of solar cell technology. It is clear from Fig. 12 that the suggested architecture achieves its maximum efficiency of 19.8 % at an affinity of 3.7 eV.

3.12. Defects effect of absorber

Improving and reducing fault density is essential for enhancing perovskite solar cells' stability and performance. Research efforts focus on understanding and mitigating defects through improved material synthesis, device engineering, and encapsulating techniques to improve PSC technology's commercial viability. Elevated defect density may result in heightened electron and hole recombination, thereby diminishing the solar cell's efficiency. Defects may act as trapping sites for charge carriers, promoting non-radiative recombination and presented in a decrease in the V_{OC} and J_{sc} [55,56]. Defects can influence the

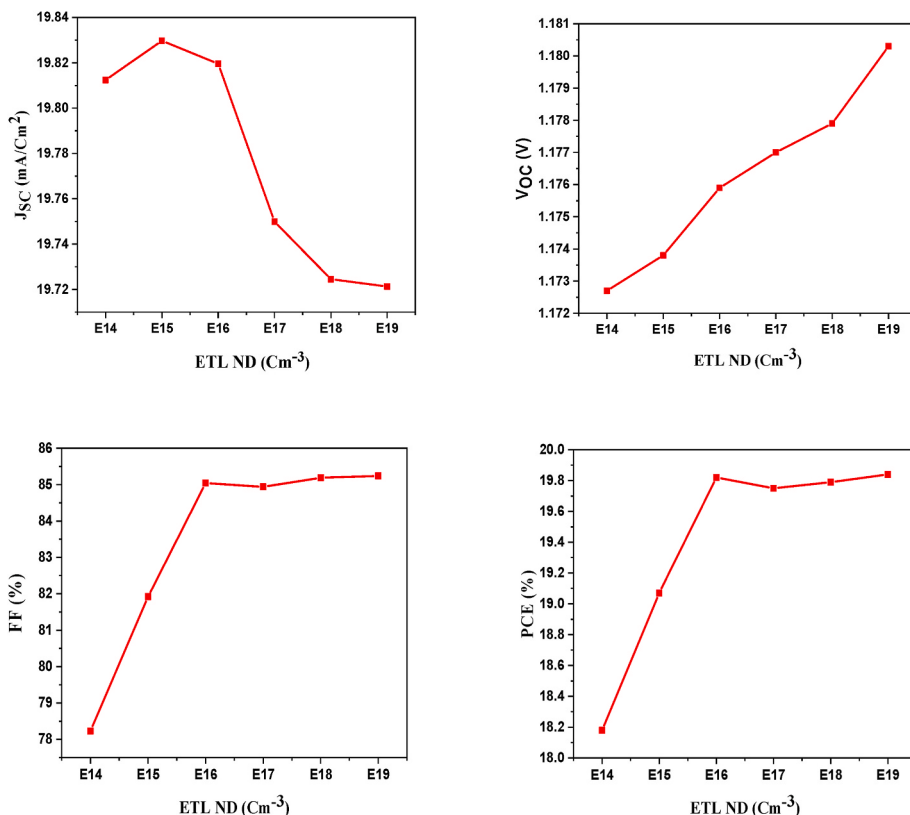


Fig. 9. Effect of Donor doping concentration of ETL film on V_{OC} ; J_{SC} ; FF; PCE.

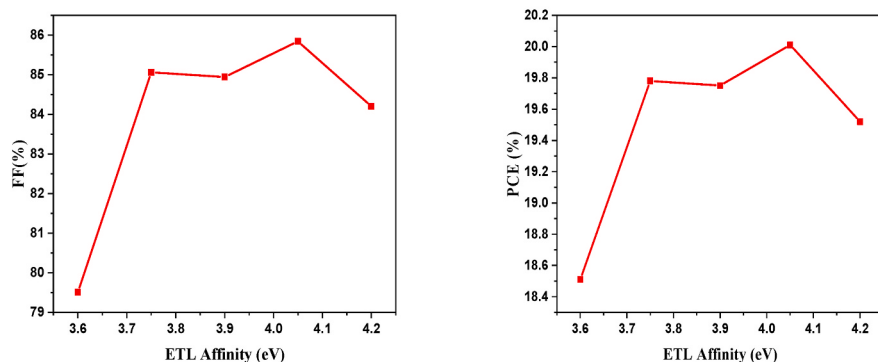
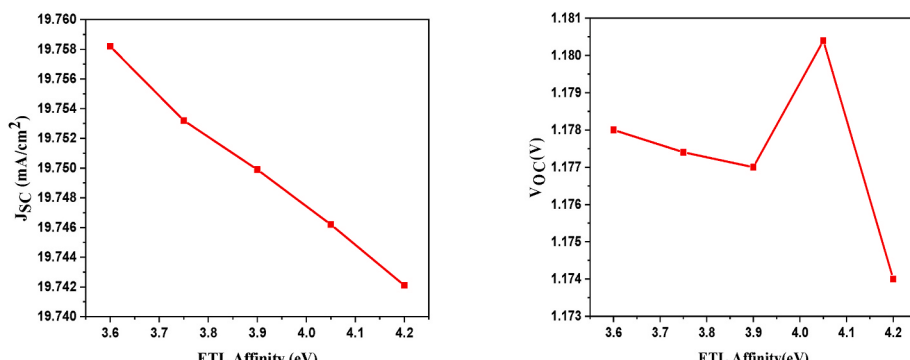


Fig. 10. Influence of Affinity (eV) of ETL material on V_{OC} ; J_{SC} ; FF; PCE.

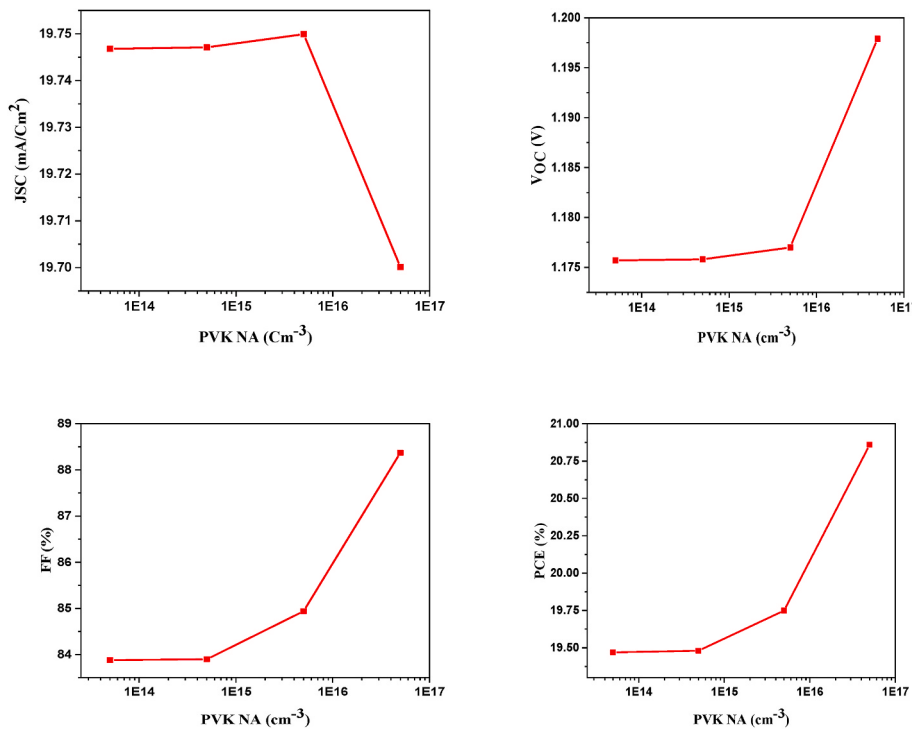
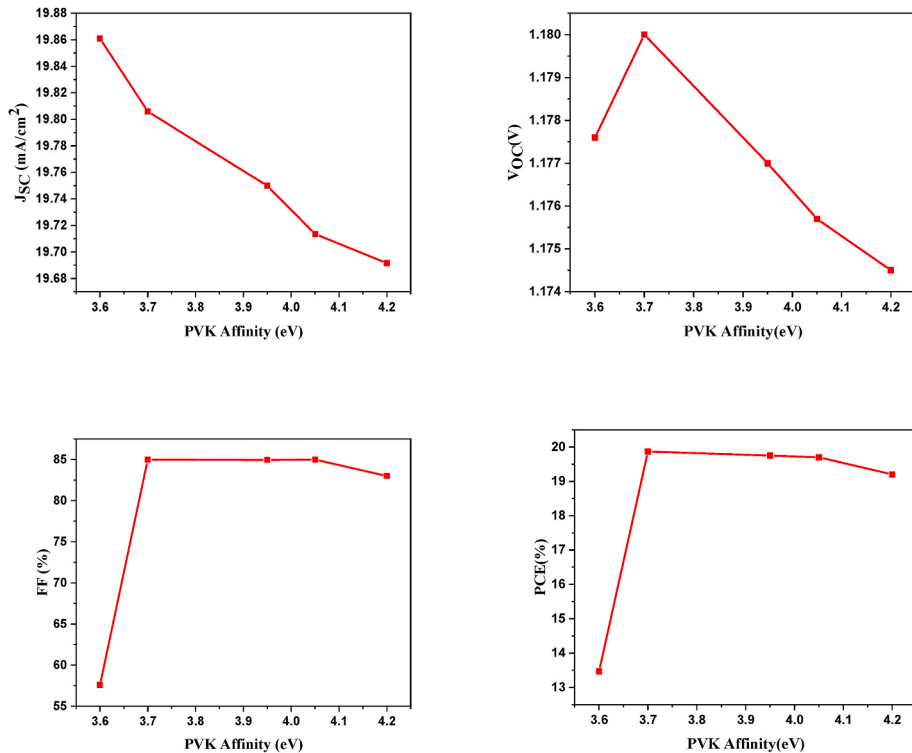


Fig. 11. Effect of acceptor doping of absorber on output parameters.

Fig. 12. Effect of Affinity x of absorber on V_{OC} ; J_{SC} ; FF; PCE.

lifetime of photogenerated carriers, affecting the duration during which carriers are available for collection. Increased defect density often correlates with shorter carrier lifetimes, impacting the PCE and performance of the solar cell. Defects can act as trap states that facilitate trap-assisted recombination of charge carriers. Trap-assisted recombination pathways can compete with radiative recombination, leading to

increased losses and reduced quantum efficiency [57,58]. Fig. 13 further illustrates how the J_{sc} , V_{oc} , FF, and PCE all sharply decrease as defect density rises. When the fault density reaches 10^{16} cm^{-3} , the efficiency almost drops to 14 % [59].

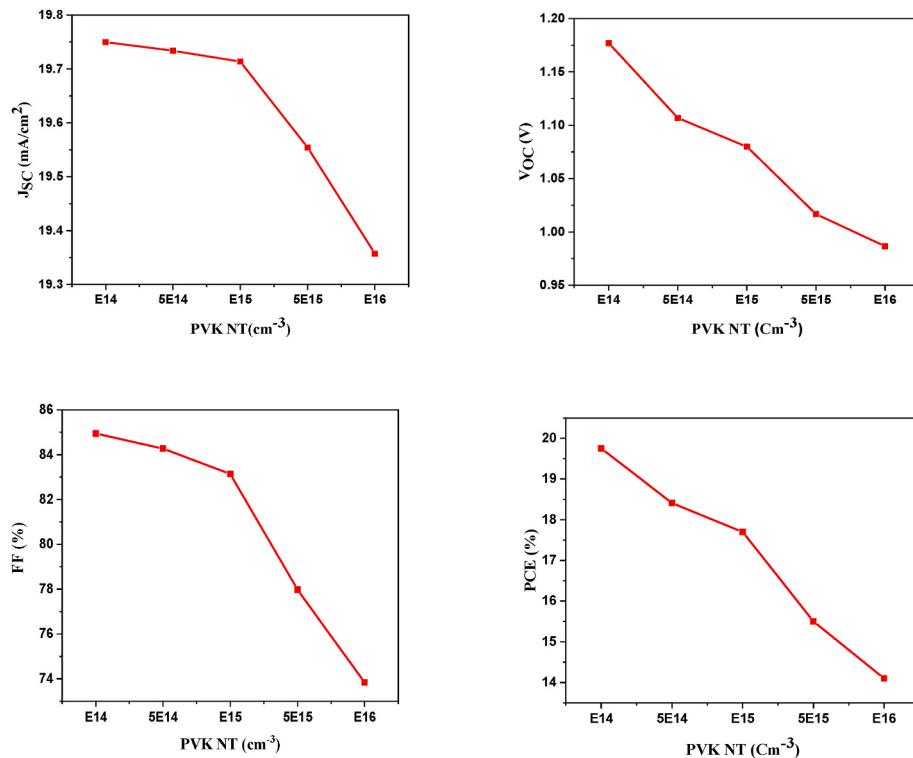


Fig. 13. Effect of Defects NT of absorber on V_{oc} ; J_{sc} ; FF; PCE.

3.13. Effect of acceptor doping of HTL

We've previously explored the significance of doping concentration in various layers of the solar cell. Fig. 14 clearly explains the substantial effect of increased acceptor doping concentration (NA) on both Voc and FF. However, this comes with a trade-off, as J_{sc} and PCE show a

significant decline. This reduction in J_{sc} and PCE is linked to greater doping levels-induced recombination and decreased carrier mobility. Notably, when NA reaches 10^{19} cm^{-3} , The solar cell's efficiency drops precipitously to 19.7 %.

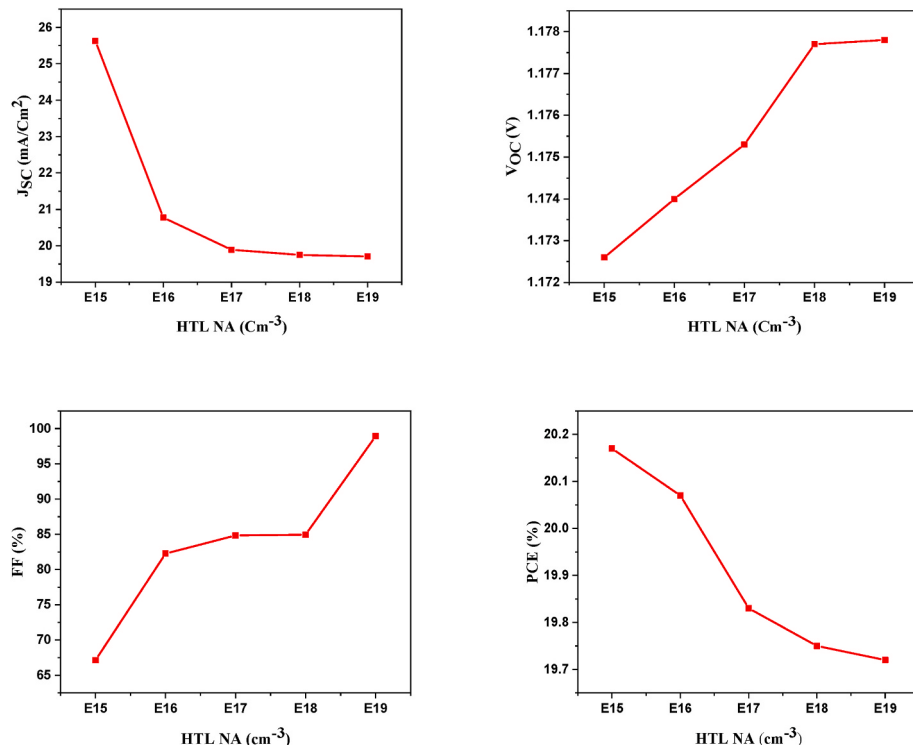


Fig. 14. Impact of acceptor doping of HTL on output parameters.

3.14. Thickness effect of ETL vs absorber

The absorber layer's thickness is directly related to light absorption. More light absorption from a larger absorber layer could result in higher photocurrent. However, excessively thick absorber layers may lead to longer charge extraction paths, impacting charge carrier gathering and rising the likelihood of recombination. The energy level alignment at the interface between the absorber layer and the ETL might be affected by the thickness of the ETL. Alignment correctly is essential for efficient charge transfer and lower losses. Thickness variations may impact the band bending and alignment, affecting the V_{OC} and overall device performance. The optimal ETL and absorber layer thicknesses depend on the specific materials used, the device architecture, and the desired performance metrics. Experimentation and optimization are typically conducted to find the right balance that maximizes light absorption, charge extraction, and overall solar cell efficiency. From Fig. 15 it is evident that for higher J_{SC} and PCE high absorber thickness is required whereas for higher V_{OC} and FF lower absorber thickness is essential. It can also be seen from Fig. 15.

3.15. Thickness effect of absorber vs HTL

Light absorption is directly correlated with the thickness of the absorber layer. Perhaps more light can be absorbed by a thicker absorber layer, helps to an increased photocurrent. However, excessively thick absorber layers may lead to longer charge extraction paths, impacting charge carrier collection and increasing the likelihood of recombination [60,61]. The energy level alignment at the interface between the absorber layer and the HTL might be affected by the thickness of the HTL. Proper alignment is crucial for effective charge transfer and reduced losses [62]. We have already discussed about all these in the absorber and ETL layer optimization section already [63,64]. From Fig. 16 it is evident that for higher J_{SC} and PCE higher PVK thickness and lower HTL thickness is essential. Similarly for higher V_{OC} and higher FF lower PVK thickness and lower HTL thickness is essential [65,66].

A performance comparison table (See Table 2) with other published

article consisting of CsSnCl_3 materials is provided here to validate the proposed model. With proper ETL and HTL combination and an optimized perovskite as well as ETL and HTL thickness the proposed model provides a higher conversion efficiency as compared to other referred literature [66–68].

4. Conclusion

In summary, an innovative hetero structure solar cell is proposed by integrating effective ETLs like CBTS and HTLs built C₆₀. Modeling outcomes demonstrate that heterostructures consisting of ITO/C₆₀/CsSnCl₃/CBTS/Au exhibit remarkable photoconversion efficiency. It is found that an affinity value of 4.05 eV, along with higher PVK thickness and lower HTL thickness is essential for higher J_{SC} and PCE. Most importantly lower defect density is essential for higher V_{OC} and high PCE. Similarly for higher V_{OC} and higher FF lower PVK thickness and lower HTL thickness is essential. With all this optimization, the proposed hetero structure provides an optimal V_{OC} of 1.18 V, a J_{SC} of 22.22 mA/cm², a FF of 87 %, and a PCE of 20.5 %. This thorough simulation analysis provides insightful information and identifies a viable path for future CsSnCl₃-based solar cell development.

CRediT authorship contribution statement

Okba Saidani: Software, Investigation, Formal analysis, Data curation, Conceptualization. **Abderrahim Yousfi:** Software, Methodology, Formal analysis. **D.P. Samajdar:** Formal analysis, Conceptualization. **Xueqing Xu:** Formal analysis. **Taye Biniyam Zemene:** Formal analysis. **Sagar Bhattarai:** Methodology, Formal analysis. **M Khalid Hossain:** Investigation, Conceptualization. **Girija Shankar Sahoo:** Methodology, Investigation, Formal analysis, Data curation, Conceptualization.

Declaration of competing interest

The authors declare that they have no known competing financial interests or personal relationships that could have appeared to influence

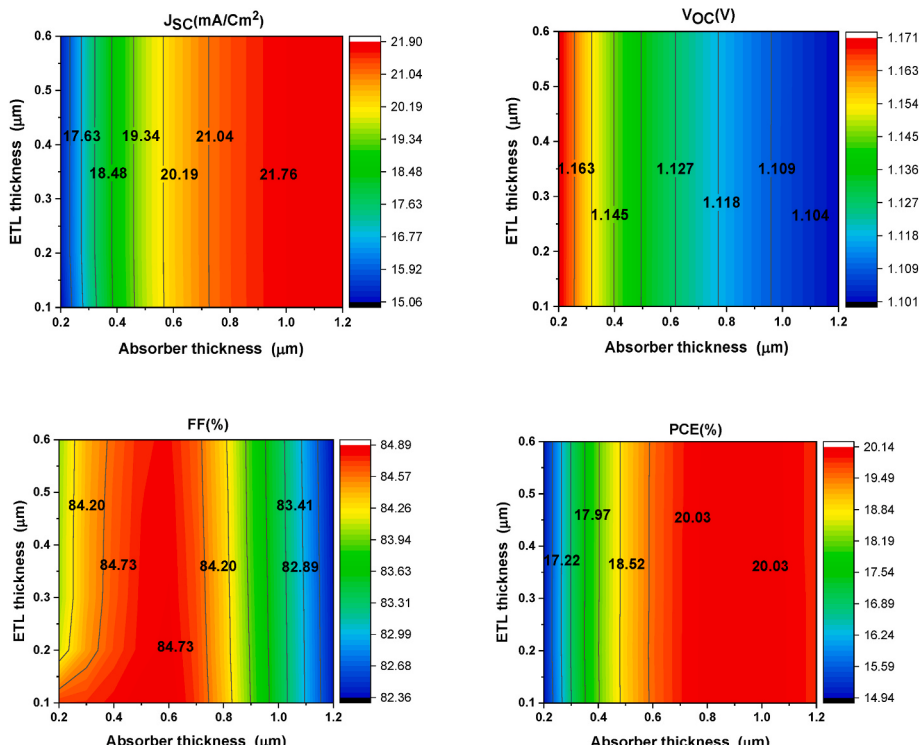


Fig. 15. Thickness effect of ETL vs absorber on V_{OC} ; J_{SC} ; FF; PCE.

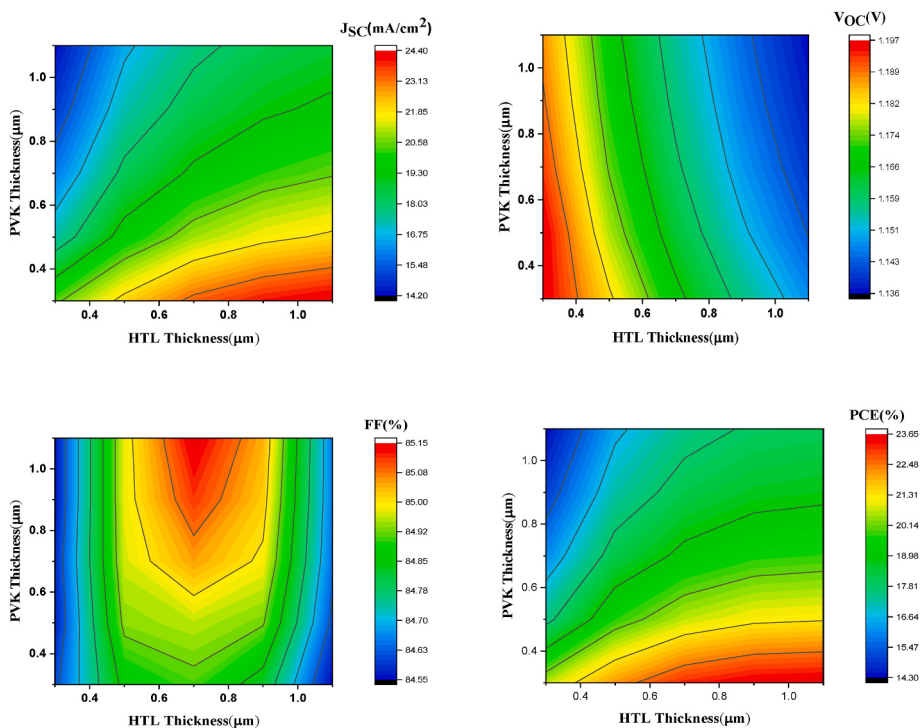


Fig. 16. Thickness effect of absorber vs HTL on V_{OC} ; J_{SC} ; FF; PCE.

Table 2
Validation of proposed model by comparing with other published literature.

Cell structure	J_{SC} (mA/cm ²)	V_{OC} (V)	FF (%)	E_{eff} (%)	Reference
ITO/TiO ₂ /CsSnCl ₃ /Cu ₂ O/Au	24.39	0.98	76.56	19.38	[66]
FTO/PCBM/CsSnCl ₃ /PTAA/Au	15.34	1.3	89.9	17.93	[67]
ITO/SnO ₂ /PbSO ₄ /CsSnCl ₃ /Spiro-OMeTAD/Au	21.682	0.909	77.045	15.195	[68]
ITO/SnO ₂ /PbCO ₃ /CsSnCl ₃ /Spiro-OMeTAD/Au	21.682	0.993	80.715	17.378	[68]
ITO/C ₆₀ /CsSnCl ₃ /CBTS/Au	22.22	1.18	87	20.5	This work

the work reported in this paper.

Data availability

Data will be made available on request.

References

- [1] A. Yousfi, O. Saidani, Z. Messai, R. Zouache, M. Meddah, Y. Belgoumri, Design and simulation of a triple absorber layer perovskite solar cell for high conversion efficiency, *East European Journal of Physics* (4) (2023) 137–146.
- [2] B. Saparov, et al., Thin-film deposition and characterization of a Sn-deficient perovskite derivative Cs₂SnI₆, *Chem. Mater.* 28 (2016) 2315–2322.
- [3] B. Lee, et al., Air-stable molecular semiconducting iodosalts for solar cell applications: Cs₂SnI₆ as a hole conductor, *J. Am. Chem. Soc.* 136 (2014) 15379–15385.
- [4] Palazon, F. et al. Polymer-free Films of Inorganic Halide Perovskite Nanocrystals as UV-To-White Color-Conversion Layers in LEDs.
- [5] W.-J. Yin, T. Shi, Y. Yan, Unique properties of halide perovskites as possible origins of the superior solar cell performance, *Adv. Mater.* 26 (2014) 4653–4658.
- [6] O. Saidani, S. Tobbeche, Numerical study and design of high-efficiency p-In_{0.1}Ga_{0.9}N/i-GaN/n-GaN heterojunction photodiode, *Micro and Nanostructures* 175 (2023) 207490.
- [7] X. Qiu, et al., From unstable CsSnI₃to air-stable Cs₂SnI₆:A lead-free perovskite solar cell light absorber with bandgap of 1.48 eV and high absorption coefficient, *Sol. Energy Mater. Sol. Cells* 159 (2017) 227–234.
- [8] X. Qiu, et al., Lead-free mesoscopic Cs₂SnI₆ perovskite solar cells using different nanostructured ZnO nanorods as electron transport layers, *Phys. Status Solidi Rapid Res. Lett.* 10 (2016) 587–591.
- [9] A. Miyata, et al., Direct measurement of the exciton binding energy and effective masses for charge carriers in organic–inorganic tri-halide perovskites, *Nat. Phys.* 11 (2015) 582–587.
- [10] T.M. Khan, A. Hosen, O. Saidani, S.R. Al Ahmed, Artificial neural network assisted numerical analysis on performance enhancement of Sb₂(S, Se) 3 solar cell with SnS as HTL, *Mater. Today Commun.* 109639 (2024).
- [11] Y. Shao, et al., Grain boundary dominated ion migration in polycrystalline organic–inorganic halide perovskite films, *Energy Environ. Sci.* 9 (2016) 1752–1759.
- [12] N. Rolston, et al., Engineering stress in perovskite solar cells to improve stability, *Adv. Energy Mater.* 8 (2018) 1802139.
- [13] W.-Q. Wu, et al., Bilateral alkylamine for suppressing charge recombination and improving stability in blade-coated perovskite solar cells, *Sci. Adv.* 5 (2019) eaav8925.
- [14] G.S. Sahoo, S. Bhattacharai, E. Feddi, M. Verma, A.N.Z. Rashed, O. Saidani, G. P. Mishra, Unveiling the potential of lead-free Cs₂AgBiBr₆ (CABB) perovskite for solar cell application, *Sol. Energy Mater. Sol. Cell.* 271 (2024) 112873.
- [15] O. Saidani, Y. Abderrahim, M. Zitouni, G.S. Sahoo, R. Zouache, M.R. Mohammad, M.K. Hossain, Numerical study of high-performance lead-free CsSnCl₃-based perovskite solar cells, *J. Opt.* 1–19 (2024).
- [16] H.-S. Kim, et al., Lead Iodide perovskite sensitized all-solid-state submicron thin film mesoscopic solar cell with efficiency exceeding 9, *Sci. Rep.* 2 (2012) 591.
- [17] M.F. Pervez, et al., Influence of total absorbed dose of gamma radiation on optical bandgap and structural properties of Mg-doped zinc oxide, *Optik* 162 (2018) 140–150.
- [18] M.M. Lee, J. Teuscher, T. Miyasaka, T.N. Murakami, H.J. Snaith, Efficient hybrid solar cells based on meso-superstructured organometal halide perovskites, *Science* 338 (2012) 643–647.
- [19] M.N.H. Mia, et al., Influence of Mg content on tailoring optical bandgap of Mg-doped ZnO thin film prepared by sol-gel method, *Results Phys.* 7 (2017) 2683–2691.
- [20] J.-G. Yu, et al., The effect of calcination temperature on the surface microstructure and photocatalytic activity of TiO₂ thin films prepared by liquid phase deposition, *J. Phys. Chem. B* 107 (2003) 13871–13879.
- [21] A. Mei, et al., A hole-conductor-free, fully printable mesoscopic perovskite solar cell with high stability, *Science* 345 (2014) 295–298.
- [22] A. Baktash, O. Amiri, A. Sasani, Improve efficiency of perovskite solar cells by using Magnesium doped ZnO and TiO₂ Compact layers, *Superlattice. Microst.* 93 (2016) 128–137.
- [23] L. Kavan, Conduction band engineering in semiconducting oxides (TiO₂, SnO₂): applications in perovskite photovoltaics and beyond, *Catal. Today* 328 (2019) 50–56.

- [24] M.F. Rahman, et al., Design and numerical investigation of cadmium telluride (CdTe) and iron silicide (FeSi2) based double absorber solar cells to enhance power conversion efficiency, *AIP Adv.* 12 (2022) 105317.
- [25] Y.H. Khattak, F. Baig, H. Toura, S. Beg, B.M. Soucase, CZTSe kesterite as an alternative hole transport layer for MASnI3 perovskite solar cells, *J. Electron. Mater.* 48 (2019) 5723–5733.
- [26] X.-F. Diao, et al., Study on the property of electron-transport layer in the doped formamidinium lead iodide perovskite based on DFT, *ACS Omega* 4 (2019) 20024–20035.
- [27] S. Bhattacharai, D. Jayan, A. Yousfi, M. Chowdhury, M.F. Rahman, R. Pandey, M. K. Hossain, Novel double graded perovskite materials for performance increment of perovskite solar cell using extensive numerical analysis, *Phys. Scripta* 98 (9) (2023) 095507.
- [28] B. Gil, et al., Recent progress in inorganic hole transport materials for efficient and stable perovskite solar cells, *Electron. Mater. Lett.* 15 (2019) 505–524.
- [29] J. Chen, N.-G. Park, Inorganic hole transporting materials for stable and high efficiency perovskite solar cells, *J. Phys. Chem. C* 122 (2018) 14039–14063.
- [30] S. Rafique, S.M. Abdullah, M.M. Shahid, M.O. Ansari, K. Sulaiman, Significantly improved photovoltaic performance in polymer bulk heterojunction solar cells with graphene oxide/PEDOT:PSS double decked hole transport layer, *Sci. Rep.* 7 (2017) 39555.
- [31] S. Wang, et al., Role of 4- tert -butylpyridine as a hole transport layer morphological controller in perovskite solar cells, *Nano Lett.* 16 (2016) 5594–5600.
- [32] C. Liu, et al., Highly stable and efficient perovskite solar cells with 22.0% efficiency based on inorganic-organic dopant-free double hole transporting layers, *Adv. Funct. Mater.* 30 (2020) 1908462.
- [33] D. Shin, et al., BaCu2Sn(S, Se)4: earth-abundant chalcogenides for thin-film photovoltaics, *Chem. Mater.* 28 (2016) 4771–4780.
- [34] R. Chakraborty, et al., Colloidal synthesis, optical properties, and hole transport layer applications of Cu2BaSnS4 (CBTS) nanocrystals, *ACS Appl. Energy Mater.* 2 (2019) 3049–3055.
- [35] T. Das, G. Di Liberto, G. Pacchioni, Density functional theory estimate of halide perovskite band gap: when spin orbit coupling helps, *J. Phys. Chem. C* 126 (2022) 2184–2198.
- [36] M. Ben Bechir, M.H. Dhaou, Study of charge transfer mechanism and dielectric relaxation of all-inorganic perovskite CsSnCl3, *RSC Adv.* 11 (2021) 21767–21780.
- [37] M.S. Ali, S. Das, Y.F. Abed, M.A. Basith, Lead-free CsSnCl3 perovskite nanocrystals: rapid synthesis, experimental characterization and DFT simulations, *Phys. Chem. Chem. Phys.* 23 (2021) 22184–22198.
- [38] M.S. Ali, S. Das, Y.F. Abed, M.A. Basith, Lead-free CsSnCl3 perovskite nanocrystals: rapid synthesis, experimental characterization and DFT simulations, *Phys. Chem. Chem. Phys.* 23 (38) (2021) 22184–22198.
- [39] J. Islam, A.K.M.A. Hossain, Narrowing band gap and enhanced visible-light absorption of metal-doped non-toxic CsSnCl3 metal halides for potential optoelectronic applications, *RSC Adv.* 10 (2020) 7817–7827.
- [40] M.I. Khalil, M.T.H. Bhuiyan, M.A. Rahman, M.S. Ali, M. Aftabuzzaman, Effects of Fe doping on the visible light absorption and bandgap tuning of lead-free (CsSnCl3) and lead halide (CsPbCl3) perovskites for optoelectronic applications, *AIP Adv.* 11 (2021) 035229.
- [41] M.I. Khalil, M.T. Hossen Bhuiyan, Effects of Cr- and Mn-alloying on the band gap tuning, and optical and electronic properties of lead-free CsSnBr3 perovskites for optoelectronic applications, *RSC Adv.* 10 (2020) 43660–43669.
- [42] M. Roknuzzaman, K. Ostrikov, H. Wang, A. Du, T. Tesfamichael, Towards lead-free perovskite photovoltaics and optoelectronics by ab-initio simulations, *Sci. Rep.* 7 (2017) 14025.
- [43] J. Ur Rehman, et al., First-principles calculations to investigate structural, electronics, optical and elastic properties of Sn-based inorganic Halide-perovskites CsSnX3 ($X = I, Br, Cl$) for solar cell applications, *Comput. Theor. Chem.* 1209 (2022) 113624.
- [44] M.H. Ali, et al., Numerical analysis of FeSi2 based solar cell with PEDOT:PSS hole transport layer, *Mater. Today Commun.* 34 (2023) 105387.
- [45] R. Pandey, et al., Halide composition engineered non-toxic perovskite-silicon tandem solar cell with 30.7% conversion efficiency, *Appl. Electron. Mater.* 5 (2023) 5303–5315.
- [46] Data retrieved from the Materials Project for CsSnCl3 (mp-27394) from database version, v2023.11.1, <https://materialsproject.org/materials/mp-27394/>.
- [47] M.K. Hossain, et al., Effect of various electron and hole transport layers on the performance of CsPbI3-based perovskite solar cells: a numerical investigation in DFT, SCAPS-1D, and wxAMPS frameworks, *ACS Omega* 7 (2022) 43210–43230.
- [48] S. Srivastava, A.K. Singh, P. Kumar, B. Pradhan, Comparative performance analysis of lead-free perovskites solar cells by numerical simulation, *J. Appl. Phys.* 131 (2022) 175001.
- [49] Y. Raoui, et al., Performance analysis of MAPbI3 based perovskite solar cells employing diverse charge selective contacts: simulation study, *Sol. Energy* 193 (2019) 948–955.
- [50] Feng, J. & Xiao, B. Effective Masses and Electronic and Optical Properties of Non-toxic MASnX3.
- [51] $X = Cl, Br$, and I) perovskite structures as solar cell absorber: a theoretical study using HSE06, *J. Phys. Chem. C* 118, 19655 19660 (2014).
- [52] M.H.K. Rubel, et al., First-principles calculations to investigate structural, elastic, electronic, thermodynamic, and thermoelectric properties of CaPd3B4O12 ($B = Ti, V$) perovskites, *Results Phys.* 42 (2022) 105977.
- [53] M.R. Islam, A.A.M. Mazumder, M.R.H. Mojumder, A.S.Z. Shifat, M.K. Hossain, Strain-induced tunable optoelectronic properties of inorganic halide perovskites APbCl3 ($A = K, Rb$, and Cs), *Jpn. J. Appl. Phys.* (2023), <https://doi.org/10.35848/1347-4065/acb09e>.
- [54] M.H.K. Rubel, et al., First-principles calculations to investigate physical properties of single-cubic (Ba $_0.82$ K $_0.18$)(Bi $_0.53$ Pb $_0.47$ O $_3$) novel perovskite superconductor, *Mater. Today Commun.* 33 (2022) 104302.
- [55] G.S. Sahoo, G.P. Mishra, Design and modelling of InGaP/GaSb tandem cell with embedded 1-D GaAs quantum superlattice, *IET Circuits, Devices Syst.* 14 (2020) 471–476.
- [56] G.S. Sahoo, G.P. Mishra, Use of hetero intrinsic layer in GaAs P-I-N solar cell to improve the intermediate band performance, *Mater. Sci. Eng. B* 263 (2021) 114862, 1–11.
- [57] G.S. Sahoo, C. Harini, N. Mahadevi, P.S. Nethra, A. Tripathy, M. Verma, G. P. Mishra, CuO film as a recombination blocking layer: a unique approach for the efficiency improvement of Si solar cells, *Silicon* 15 (2023) 4039–4048.
- [58] N.E. Ouarie, J.E. hamdaoui, G.S. Sahoo, K.G. Rodriguez-Osorio, M. Courel, M. Zazoui, L. M Pérez, D. Laroze, E. Feddi, Modelling of highly efficient cngs based kesterite solar cell: a DFT study along with SCAPS-1D analysis, *Sol. Energy* 263 (2023) 111929.
- [59] G.S. Sahoo, M. Verma, S. Routray, G.P. Mishra, Unveiling the effect of CZTSSe quantum superlattice on the interfacial and optical properties of CZTS kesterite solar cell, *IEEE Trans. Nanotechnol.* 23 (2024) 286–292.
- [60] L. Lin, et al., Simulated development and optimized performance of CsPbI3 based all-inorganic perovskite solar cells, *Sol. Energy* 198 (2020) 454–460.
- [61] K.D. Jayan, V. Sebastian, J. Kurian, Simulation and optimization studies on CsPbI3 based inorganic perovskite solar cells, *Sol. Energy* 221 (2021) 99–108.
- [62] T.M. Khan, A. Hosen, O. Saidani, S.R. Al Ahmed, Artificial neural network assisted numerical analysis on performance enhancement of Sb2 (S, Se) 3 solar cell with SnS as HTL, *Mater. Today Commun.* 109639 (2024).
- [63] W.A. Saidi, S. Poncé, B. Monserrat, Temperature dependence of the energy levels of methylammonium lead iodide perovskite from first-principles, *J. Phys. Chem. Lett.* 7 (2016) 5247–5252.
- [64] M.K. Hossain, G.I. Toki, A. Kuddus, M.H.K. Rubel, M.M. Hossain, H. Bencherif, M. Mushtaq, An extensive study on multiple ETL and HTL layers to design and simulation of high-performance lead-free CsSnCl3-based perovskite solar cells, *Sci. Rep.* 13 (2023) 2521.
- [65] M.K. Hossain, G.I. Toki, A. Kuddus, M.K. Mohammed, R. Pandey, J. Madan, D. P. Samajdar, Optimization of the architecture of lead-free CsSnCl3-perovskite solar cells for enhancement of efficiency: a combination of SCAPS-1D and wxAMPS study, *Mater. Chem. Phys.* 308 (2023) 128281.
- [66] S. Rawat, J. Madan, R. Pandey, Optimizing the efficiency and stability of CsSnCl3-based perovskite solar cells using SCAPS simulation tool, in: 2023 4th International Conference for Emerging Technology (INCET), 2023, pp. 1–4.
- [67] S. Srivastava, A.K. Singh, P. Kumar, B. Pradhan, Comparative performance analysis of lead-free perovskites solar cells by numerical simulation, *J. Appl. Phys.* 131 (2022) 175001.
- [68] G. Lei, B. Zhang, X. Cheng, R. Xia, T. Liu, W. Zhao, Interfacial engineering dominated passivation strategy to facilitate performance improvement of CsSnCl3 PSCs by induced Sn–O bonds: insight from DFT calculations and device simulations, *Chem. Eng. J.* 153886 (2024), <https://doi.org/10.1016/j.cej.2024.153866>.